From two-dimensional electron gas to localized charge: Dynamics of polaron formation in organic semiconductors

Ti Wang, Claudiu Caraiani, G. William Burg, and Wai-Lun Chan

Phys. Rev. B **91**, 041201 — Published 9 January 2015

DOI: 10.1103/PhysRevB.91.041201

From two-dimensional electron gas to localized charge: dynamics of polaron formation in organic semiconductors

Ti Wang, Claudiu Caraiani, G. William Burg, Wai-Lun Chan*

Department of Physics and Astronomy, University of Kansas, Lawrence, KS 66045

* wlchan@ku.edu

Abstract:

Electronic transport in organic semiconductors is mediated by localized polarons. However, the dynamics on how delocalized electrons collapse into polarons through electron-nuclear interaction is not well-known. In this work, we use time and angle resolved photoemission spectroscopy (TR-ARPES) to study polaron formation in titanyl phthalocyanine deposited on Au(111) surfaces. Electrons are optically excited from the metal to the organic layer via the image potential state, which evolves from a dispersive to a non-dispersive state after photoexcitation. The spatial size of the electrons is determined from the band-structure using a tight-binding model. It is observed that the two-dimensional electron wave collapses into a wave packet of size ~ 3 nm within 100 fs after photoexcitation.

PACS: 73.20.-r, 79.60.Dp, 71.38.-k, 78.47.J-

In organic semiconductors, electrons and holes are dressed by the nuclear motion of molecules, resulting in the formation of localized quasiparticles named polaron [1]. Experiments resolving polaron formation dynamics in detail will enable us to better understand the interplay between electron-electron and electron-vibrational interactions. These fundamental interactions control properties and processes, such as charge mobility [2,3], charge trapping [4], and interfacial transport [5], which in turn determine the performances of various optoelectronic devices. For example, it is recently proposed that electron delocalization can assist charge separation in organic photovoltaics [6-10]. However, how this mechanism can be better utilized is not clear. Therefore, there is a critical need in developing experimental tools that can unveil these dynamic processes at the molecular level.

In this work, we use time- and angle-resolved photoemission spectroscopy (TR-ARPES) to study the polaron formation dynamics by optically-injecting electrons from metals to organic semiconductors via the image potential state (IPS). IPS is a two-dimensional (2-D) surface state in which the electron is bound by an image charge that locates underneath a polarizable surface [11]. For metal/adsorbate systems, IPS is located near the adsorbate's surface [12]. Similar to charges in adsorbate's unoccupied states, electrons in IPS are subject to electron-vibrational interactions and the dielectric environment originated from the adsorbates. These interactions can lead to dynamic localization of the IPS, which has been studied by TR-ARPES in systems such as alkanes and polar solvents on metal surfaces [13-16], ionic liquids [17], and ionic crystals [18]. Recently, TR-ARPES has been used to study 2-D states at organic/metal interfaces [19-21] and organic semiconductor surfaces [22-25]. However, in most of the works on organic semiconductors, no temporal evolution of band structure has been observed. On α-sexithiophene surfaces, Johns *et al.* found that the effective mass of the IPS band increases with increasing time

[26]. However, no high resolution ARPES spectrum was reported. In this work, we use titanyl phthalocyanine (TiOPc) as a model system to study polaron formation in organic crystals. By modeling the measured band structure with a tight-binding model, we determine the temporal evolution of the spatial size of electrons when they collapse from delocalized waves into localized polarons.

TiOPc were deposited on a Au(111) substrate by thermal evaporation. The Au(111) surface was prepared by sputtering (~5 μA, 20 min.) and annealing (800 K, 40 min.) cycles. The TiOPc molecules (Luminescence Technology, >99%) were deposited at room temperature at a rate of 0.5 Å/min. The film thickness was monitored by a quartz crystal microbalance. After the deposition, the sample was transferred to another chamber (base pressure < 1×10^{-10} Torr) under UHV environment where TR-ARPES experiments were performed. TiOPc molecules can be grown epitaxially on the Au(111) surface [27] where the molecules are arranged in a square lattice with a face-on orientation. The crystallinity of our sample was verified *in-situ* by the low energy electron diffraction. Photoemission experiments were done at a sample temperature of 120 K. The sample was excited by two laser pulses with a controllable time-delay between pulses. The first pulse ($h\upsilon_1$) had a photon energy of 4.43 eV (pulse energy ~ 10 nJ, pulse duration ~ 55 fs), which was created by frequency doubling the output of a non-collinear optical parametric amplifier (NOPA, ORPHEUS-N-3H, Light Conversion). The second pulse ($h\upsilon_2$) had a photon energy of 1.75 eV (energy ~ 280 nJ, duration ~ 25 fs), which was generated by another NOPA (ORPHEUS-N-2H, Light Conversion). Both NOPAs were pumped by a Yb:KGW regenerative amplifier running at 500 kHz (PHAROS, Light Conversion). The kinetic energy (KE) and emission angle of photoelectrons were detected by a hemispherical electron energy analyzer (Phoibos 100, SPECS).

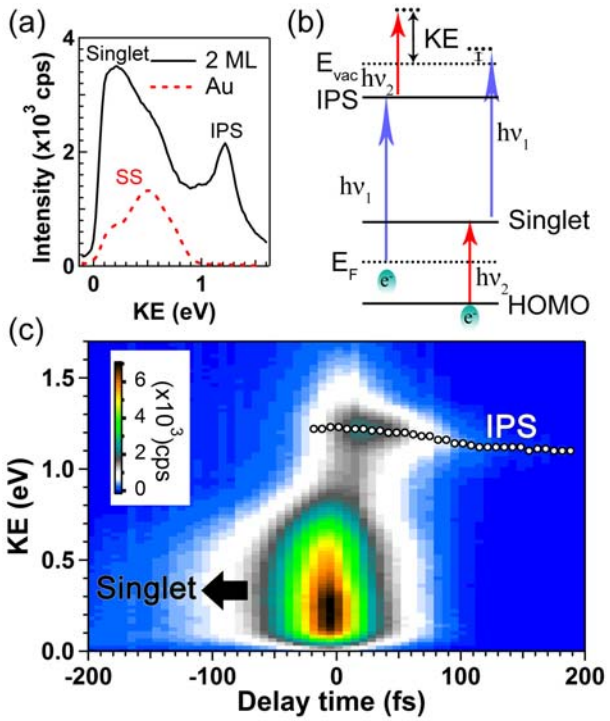

FIG. 1: (a) Photoemission spectrum at t = 20 fs for a 2 ML TiOPc sample. The dotted line represents the spectrum of Au(111). (b) Energy level diagram for the TiOPc/Au(111) interface ($h\nu_1$ = 1.75 eV; $h\nu_2$ = 4.43 eV) (c) Time-resolved spectrum for the 2 ML sample. The emission angle of electrons is 0°.

Figure 1a shows the spectrum for a 2 monolayer (ML) thick sample at delay time (t) equal to 20 fs. A positive delay time represents the UV pulse preceding the visible pulse. Two peaks can be identified. The peak with lower energy represents the singlet state [10] which is populated by the visible pulse and probed by the UV pulse (Fig. 1b). In the time-resolved spectrum (Fig. 1c), this peak appears at $t < 0$. The higher energy peak can be identified as the IPS. Contrary to the singlet state, it is populated by the UV pulse and probed by the visible pulse (Fig. 1b). For comparison, a spectrum for bare Au(111) surface is shown in Fig. 1a. Only the occupied surface state (SS) of Au [28], but no IPS, can be identified. Since a bare Au(111) surface has a larger work function, our UV pump photons do not have enough energy to excite the IPS.

The binding energy of the IPS relative to the vacuum level (E_v) for 1, 2, and 3 ML of TiOPc is 0.81, 0.53, and 0.50 eV respectively. Similar binding energies are reported for IPS found on other phthalocyanine surfaces [22-24]. The binding energy decreases with the increase

of film thickness, which is consistent with the IPS located farther away from the metal substrate [29]. Figure 1c shows the time-resolved spectrum for the 2 ML sample. The color-scale represents the photoemission intensity. The IPS peak shifts to a lower energy with the increase of t (white dots), which can be explained by the localization of the IPS. Figure 2 shows the intensity and the energy of the IPS for the 2 ML sample. The lifetime of the IPS for 1, 2 and 3 ML of TiOPc is 26 fs, 38 fs, and 45 fs respectively. The thicker film has a longer lifetime, which is due to a weaker electronic coupling with the metal substrate [11]. In the 2 ML sample, the binding energy decreases by 0.11 eV in the first ~100 fs and remains stable thereafter. Similar peak shift is found for the 1 ML sample with a larger shift in energy (0.18 eV).

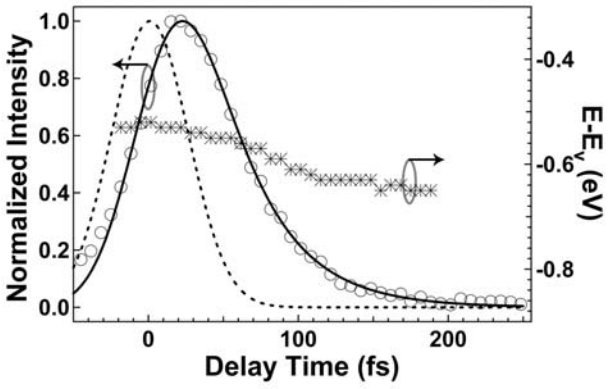

FIG. 2: The population and binding energy of the IPS as a function of time for the 2 ML sample. The dashed line represents the instrumental response function. The solid line represents the fitting to an exponential decay with a lifetime = 38 fs.

In order to understand the relaxation dynamics, we measure the angle resolved spectra at various t for the 2 ML sample, which are shown in Fig. 3. For $t \leq 40$ fs (Fig. 3a), the IPS band is essentially parabolic, indicating that the IPS is delocalized. Fitting with a parabolic dispersion (solid line in Fig. 3d) yields an effective mass of 1.6 m_e (m_e is the free electron mass). This is consistent to previous studies [22,24] in which effective masses are found in the range of 1.0 – 2.2 m_e. The spectra at later times are shown in Fig. 3b and c. The electron emission angle can be converted to the parallel momentum k of electrons as outlined in Ref. [30]. Figure 3d shows the energy-momentum dispersions at various t. Energetic positions of the peak are shown up to the k

value where a peak can still be identified. Near the band bottom (k = 0), both the energy and curvature of the band decreases with increasing t. However, the band seems to be 'pinned' at large k near and beyond the Brillouin zone (BZ) boundary (vertical line in Fig. 3d). At t = 180 fs (Fig. 3c), only a non-dispersive state is observed. The intensity distribution of this non-dispersive state in k-space has a limited width (insert in Fig. 3c). Such an evolution from dispersive to non-dispersive behavior cannot be observed in IPS on metal surfaces [11] and is related to the molecules. The observation can be explained by electron localization [12-18,26]. Similar temporal change in the band structure is found for the 1 ML sample.

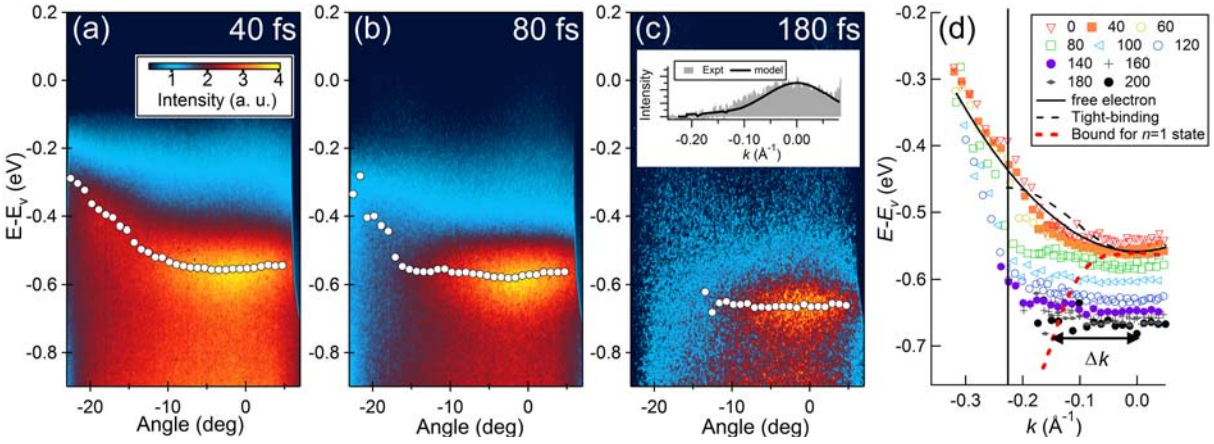

FIG. 3: TR-ARPES spectra at t equal to (a) 40 fs, (b) 80 fs, and (c) 180 fs obtained from a 2 ML sample. The insert in (c) is the intensity distribution of the localized IPS as a function of k. (d) Dispersion relationships for the IPS at various t. The delay times, which are in fs, are indicated in the legend. The vertical line is the BZ boundary.

Previous studies have shown that periodic potential introduced by the molecular layer can cause gap opening and band splitting at the BZ boundary [22,24]. We cannot resolve this splitting potentially because of the larger bandwidth of our laser pulses. However, as it will be discussed, because the localization mainly affects states near k = 0, we will focus at the band bottom. In order to understand how localization affects the band structure, the system is modeled with a tight-binding Hamiltonian:

$$\mathcal{H} = \sum_i(\varepsilon_i + \Delta\varepsilon(x))|i><i| + \sum_{i,j,i\neq j} V|i><j|. \quad (1)$$

The index i represents the molecular site i, $|i\rangle$ is the electron orbital at that site, and x is the spatial coordinate. The site energy is represented by ε_i, which is taken to be constant (ε_0) throughout the chain. The second summation represents electronic coupling between neighboring sites (i, j) with V being the electronic coupling constant. Similar Hamiltonian is commonly used to model band structure in molecular crystals [31]. The TiOPc lattice has a four-folded in-plane symmetry and domains can have three possible orientations on the Au(111) surface. Since the measured band-structure is an average of these three orientations, it is rather isotopic along different in-plane directions. Therefore, for simplicity, a 1-D model is used. For $\Delta\varepsilon(x) = 0$, the eigenstates of the Hamiltonian are delocalized Bloch's waves $|\psi_k\rangle$ with dispersion relationship given by $E(k) = \varepsilon_0 - 2V\cos ka$, where a is the lattice constant. For our system, a = 1.4 nm [27]. By fitting the dispersion relationship at t < 40 fs within the first BZ (dashed line in Fig. 3d), V is estimated to be 24 meV.

To understand how energy relaxation at local sites leads to spatial localization of electrons, we add a negative $\Delta\varepsilon(x)$ term to the site energy, which mimics energy relaxation (a potential well) induced by electron-vibrational interaction [1]. The spatial dependence of $\Delta\varepsilon(x)$ is described empirically using a Gaussian function:

$$\Delta\varepsilon(x) = -\varepsilon_1 \exp(-x^2/2{x_0}^2). \quad (2)$$

Here, ε_1 and x_0 are the amplitude and width of the potential well respectively. We choose x_0 such that the full-width half maxima (fwhm) of the potential well equal to 5 molecular sites (x_0 = 2.97 nm). We will justify this choice later. Physically, x_0 represents the size of the dynamic defect. The rather small x_0 is consistent with the conventional picture of polaron formation, in which

localization is triggered by local distortions of crystal lattice [1]. Eigenstates are determined by diagonalizing the Hamiltonian. The chain is chosen to have 701 sites and periodic boundary condition is employed.

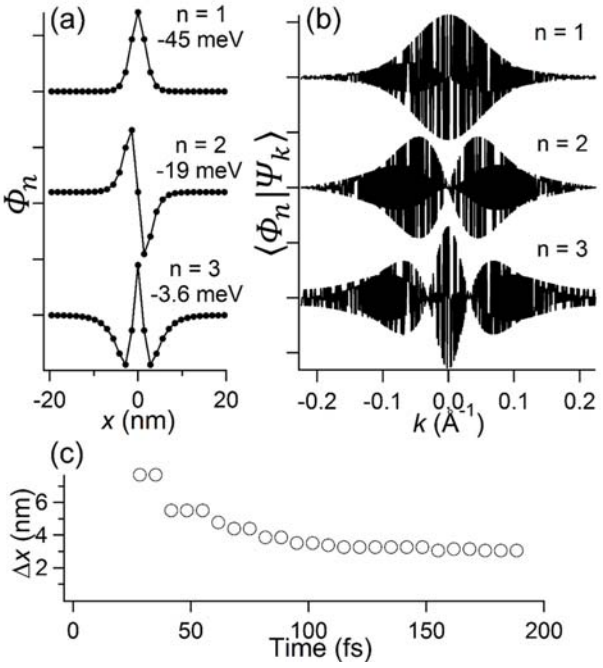

FIG. 4: (a) The wavefunction of the three localized states for ε_1 = 70 meV and x_0 = 2.97 nm. The energies with respect to the band bottom (ΔE) are indicated. (b) The localized states projected into the basis of the delocalized Bloch's waves. (c) The size of the polaron as a function of time is determined by using the data shown in Fig. 2.

For $\varepsilon_1 > 0$, localized states with energies less than $E_0 = \varepsilon_0 - 2V$ (the bottom of the delocalized band) are formed. For example, at ε_1 = 70 meV and x_0 = 2.97 nm, three localized states $|\Phi_n\rangle$ are found which are shown in Fig. 4a. The energy of these eigenstates E_n with respect to E_0 ($\Delta E = E_n - E_0$) is indicated. All these states are non-dispersive, but they have different amplitude distributions in k-space. Figure 4b shows the amplitude as a function of k when the wavefunctions are projected into the basis of the delocalized Bloch's waves $|\psi_k\rangle$. We first focus on the lowest energy eigenstate (n = 1). The energy of this localized state and, hence, ΔE is lowered if ε_1 in Eq. (2) is increased. Furthermore, the wavefunction is more localized for larger ε_1, which results in a wider spread of the probability amplitude in k-space. By varying ε_1 as a parameter, we can obtain a relationship between the eigenenergy $E_{n=1}$ and the width of the

amplitude distribution (Δk). The parameter x_0 in Eq. (2) is chosen such that the envelope of the amplitude distribution from the model matches the measured intensity distribution of the localized state in k-space at a large delay time (t = 180 fs, insert in Fig. 3c). The width Δk as a function of eigenstate energy ($E_{n=1}$) is indicated by the red dashed line in Fig. 3d. Here, Δk is defined as the 2σ width of the n = 1 state. The dashed line represents a bound to a region in k-space in which photoemission intensity originated from the n = 1 state should reside. This agrees with the experiment in which the band structure within this region is appeared to be non-dispersive.

Outside this bound, the intensity can be contributed by either the higher order non-dispersive (quantum well) states (e.g. n = 2, 3 in Fig. 4), or from the delocalized states. The higher order quantum well states are noticeable, e.g. at intermediate times (t ~ 80 – 100 fs), where a slightly higher energy plateau can be observed at $|k|$ ~ 0.1-0.2 $Å^{-1}$ (Fig. 3d). Since these localized states are closely spaced, they can be smeared out by each other and form an apparently continuous band structure [32]. At longer delay times (t ~ 200 fs), all electrons relax to the n = 1 state and only a single non-dispersive state is observed. Furthermore, states near the BZ boundary are delocalized waves with wavelength on the order of the lattice spacing. These states are barely mixed by a localized potential well (Eq. 2) and resemble the Bloch's waves of the unperturbed Hamiltonian (ε_1 = 0). Hence, the band is appeared to be 'pinned' near the BZ boundary.

A quantity that is of interest is the spatial size of the electron as a function of time. Our model cannot predict time-dependent behaviors and the underlying localization mechanism. However, we can use our model to relate experimentally measured ΔE and Δk to the spatial size (Δx) of the electron in real space. We start with the measured time dependence of ΔE (Fig. 2) and

our model is used to determine the corresponding Δx at each ΔE. As a demonstration, only the n = 1 state is considered. This state has the strongest photoemission intensity (Fig. 3b), indicating that it has the highest population when electrons are relaxing towards lower energy states. Curves such as the one shown in Fig. 4a (top panel) are fitted with a Gaussian function and Δx is defined as the fwhm of the wavefunction. The evolution of Δx as a function of t is shown in Fig. 4c. The spatial size of the electron decreases rapidly in the first 100 fs and becomes 2 - 3 nm (~ 2 molecular sites) at large t. The total relaxation energy is 110 meV. For comparison, a recent electron spin resonance measurement deduces that polarons in pentacene crystals have sizes = 1.5 and 5 molecular sites, with relaxation energies = 140 and 22 meV respectively [33]. Until now, it is implied that the observed localization is driven by electron-vibrational interaction. However, we note that other mechanisms would induce similar observations. For instance, localization can be induced by electron-electron interactions such as bipolaron formation, which is proposed to occur in pi-conjugated polymers [34]. Second, electrons can be localized by forming excitons with holes resided underneath the surface. However, it is less likely the case because the exciton binding energy in similar systems is around 0.5 eV [35].

By using TR-ARPES, we measure the temporal evolution of the band structure of the IPS on organic semiconductor surfaces, which unveils the localization of a 2D electron gas into a polaron. The spatial size of the electron is determined as a function of time from the band structure using a tight binding model. Our method gives a comprehensive view on the temporal evolution of both energy and spatial size of electrons during localization, which can be used to understand the polaron formation process in organic semiconductors. The work is supported by US National Science Foundation, grant DMR-1351716.

REFERENCE

[1] T. Holstein, Ann. Phys. **8**, 325 (1959).
[2] D. Beljonne, J. Cornil, H. Sirringhaus, P. J. Brown, M. Shkunov, R. H. Friend, and J.-L. Brédas, Adv. Funct. Mater. **11**, 229 (2001).
[3] A. Troisi, Adv. Mater. **19**, 2000 (2007).
[4] L. G. Kaake, P. F. Barbara, and X.-Y. Zhu, J. Phys. Chem. Lett. **1**, 628 (2010).
[5] Y. Xia, W. Xie, P. P. Ruden, and C. D. Frisbie, Phys. Rev. Lett. **105**, 036802 (2010).
[6] A. J. Barker, K. Chen, and J. M. Hodgkiss, J. Amer. Chem. Soc. **136**, 12018 (2014).
[7] A. A. Bakulin, A. Rao, V. G. Pavelyev, P. H. M. van Loosdrecht, M. S. Pshenichnikov, D. Niedzialek, J. Cornil, D. Beljonne, and R. H. Friend, Science **335**, 1340 (2012).
[8] S. M. Falke, C. A. Rozzi, D. Brida, M. Maiuri, M. Amato, E. Sommer, A. De Sio, A. Rubio, G. Cerullo, E. Molinari, and C. Lienau, Science **344**, 1001 (2014).
[9] L. G. Kaake, C. Zhong, J. A. Love, I. Nagao, G. C. Bazan, T.-Q. Nguyen, F. Huang, Y. Cao, D. Moses, and A. J. Heeger, J. Phys. Chem. Lett. **5**, 2000 (2014).
[10] T. Wang and W.-L. Chan, J. Phys. Chem. Lett. **5**, 1812 (2014).
[11] P. M. Echenique, R. Berndt, E. V. Chulkov, Th. Fauster, A. Goldmann, and U. Höfer, Surf. Sci. Rep. **52**, 219 (2004).
[12] X.-Y. Zhu, Surf. Sci. Rep. **56**, 1 (2004).
[13] N.-H. Ge, C. M. Wong, R. L. Lingle Jr, J. D. McNeill, K. J. Gaffney, and C. B. Harris, Science **279**, 202 (1998).
[14] A. D. Miller, I. Bezel, K. J. Gaffney, S. Garrett-Roe, S. H. Liu, P. Szymanski, and C. B. Harris, Science **297**, 1163 (2002).
[15] B. Li, J. Zhao, K. Onda, K. D. Jordan, J. Yang, and H. Petek, Science **311**, 1436 (2006).
[16] J. Stähler, M. Mehlhorn, U. Bovensiepen, M. Meyer, D. O. Kusmierek, K. Morgenstern, and M. Wolf, Phys. Rev. Lett. **98**, 206105 (2007).
[17] E. A. Muller, M. L. Strader, J. E. Johns, A. Yang, B. W. Caplins, A. J. Shearer, D. E. Suich, and C. B. Harris, J. Amer. Chem. Soc. **135**, 10646 (2013).
[18] M. Muntwiler and X.-Y. Zhu, Phys. Rev. Lett. **98**, 246801 (2007).
[19] C. H. Schwalb, S. Sachs, M. Marks, A. Schöll, F. Reinert, E. Umbach, and U. Höfer, Phys. Rev. Lett. **101**, 146801 (2008).
[20] M. Marks, N. L. Zaitsev, B. Schmidt, C. H. Schwalb, A. Schöll, I. A. Nechaev, P. M. Echenique, E. V. Chulkov, and U. Höfer, Phys. Rev. B **84**, 081301 (2011).
[21] B. W. Caplins, D. E. Suich, A. J. Shearer, and C. B. Harris, J. Phys. Chem. Lett. **5**, 1679 (2014).
[22] R. Yamamoto, T. Yamada, M. Taguchi, K. Miyakubo, H. S. Kato, and T. Munakata, Phys. Chem. Chem. Phys. **14**, 9601 (2012).
[23] M. Shibuta, K. Yamamoto, K. Miyakubo, T. Yamada, and T. Munakata, Phys. Rev. B **81**, 115426 (2010).
[24] B. W. Caplins, A. J. Shearer, D. E. Suich, E. A. Muller, and C. B. Harris, Phys. Rev. B **89**, 155422 (2014).
[25] W.-L. Chan, J. Tritsch, A. Dolocan, M. Ligges, L. Miaja-Avila, and X.-Y. Zhu, J. Chem. Phys. **135**, 031101 (2011).
[26] J. E. Johns, E. A. Muller, J. M. J. Frechet, and C. B. Harris, J. Amer. Chem. Soc. **132**, 15720 (2010).
[27] S. C. B. Mannsfeld and T. Fritz, Phys. Rev. B **71**, 235405 (2005).

[28] E. V. Chulkov, M. Machado, and V. M. Silkin, Vacuum **61**, 95 (2001).
[29] W. Berthold, P. Feulner, and U. Höfer, Chem. Phys. Lett. **358**, 502 (2002).
[30] M. Hengsberger, F. Baumberger, H. J. Neff, T. Greber, and J. Osterwalder, Phys. Rev. B **77**, 085425 (2008).
[31] M. Pope and C. E. Swenberg, *Electronic processes in organic crystals and polymers* (Oxford University Press, New York, 1999).
[32] F. Baumberger, M. Hengsberger, M. Muntwiler, M. Shi, J. Krempasky, L. Patthey, J. Osterwalder, and T. Greber, Phys. Rev. Lett. **92**, 196805 (2004).
[33] H. Matsui, A. S. Mishchenko, and T. Hasegawa, Phys. Rev. Lett. **104**, 056602 (2010).
[34] T. Koyama, A. Nakamura, and H. Kishida, ACS Photonics **1**, 655 (2014).
[35] M. Muntwiler, Q. Yang, W. A. Tisdale, and X.-Y. Zhu, Phys. Rev. Lett. **101**, 196403 (2008).